ACS OMEGA

http://pubs.acs.org/journal/acsodf

Article

Toward a SERS Diagnostic Tool for Discrimination between Cancerous and Normal Bladder Tissues via Analysis of the Extracellular Fluid

Edvinas Zacharovas, Martynas Velička,* Gediminas Platkevičius, Albertas Čekauskas, Arūnas Želvys, Gediminas Niaura,* and Valdas Šablinskas

Cite This: *ACS Omega* 2022, 7, 10539−10549

Read Online

ACCESS | Metrics & More | Article Recommendations | Supporting Information

ABSTRACT: Vibrational spectroscopy provides the possibility for sensitive and precise detection of chemical changes in biomolecules due to development of cancers. In this work, label-free near-infrared surface enhanced Raman spectroscopy (SERS) was applied for the differentiation between cancerous and normal human bladder tissues via analysis of the extracellular fluid of the tissue. Specific cancer-related SERS marker bands were identified by using a 1064 nm excitation wavelength. The prominent spectral marker band was found to be located near 1052 cm^{-1} and was assigned to the C−C, C−O, and C−N stretching vibrations of lactic acid and/or cysteine molecules. The correct identification of 80% of samples is achieved with even limited data set and could be further improved. The further development of such a detection method could be implemented in clinical practice for the aid of surgeons in determining of boundaries of malignant tumors during the surgery.

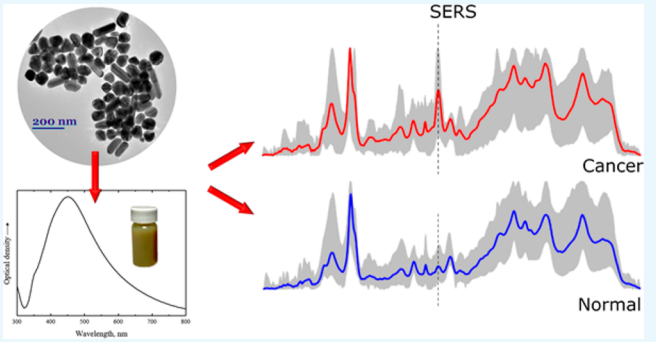

1. INTRODUCTION

Bladder cancer (BC) is the 11th most commonly diagnosed cancer for both genders. Higher rates of age-standardized incidence are observed in males comparing to females (9.0 and 2.2 per 100 000 person/years, respectively).[1] The 5-year recurrence and progression rates depend on clinical and pathological factors and vary from 31% to 78% and from 0.8% to 45%, respectively.[2] Because of the high recurrence rate and complexity of the invasive diagnostic procedures, bladder cancer has the largest economic burden to treat per patient over their lifetimes.[3] BC is commonly diagnosed by white light cystoscopy (WLC), followed by a bladder tissue biopsy. Although, WLC is widely used, it has limitations on detecting small malignant tumors, particularly sessile carcinoma in situ (CIS). Photodynamic diagnosis (PDD), with "blue" light after addition of 5-aminolaevulinic acid (ALA) or hexaminolaevulinic acid (HAL), has higher rates of sensitivity than WLC (92% vs 71%). However, its specificity is significantly lower than that of WLC (63% vs 81%), as false-positive results may be easily produced by bladder inflammation (cystitis), due to similar macroscopical appearances in some cases.[4] Samples of bladder tissue biopsy are examined by pathologists, and diagnosis is given according to BC histological criteria. The most common histological type of BC is urothelial carcinoma (UC), with approximately 90% of all cases. The remaining ∼10% of cases consist of squamous cell carcinoma, adenocarcinoma, and small cell carcinoma.[5] Since 2004, when new pathological grading system was introduced, low-grade (LG) and high-grade (HG) categories were implemented to define tumor differentiation. High-grade tumors are less differentiated and encompass all G3 and part of the G2 entities from the previous classification.[6] Although, to date, WLC is a good standard of BC diagnosis, it has a factor of subjectivity during both endoscopy and the pathological examination of the biopsy sample. It also requires repeated invasive procedures and has a high expense rate per patient. Therefore, there is need for a new accurate, noninvasive, and low-cost diagnostic method. Recently, new magnetic resonance imaging possibilities have been described with a completely new standardized reporting system (VI-RADS).[7,8] While, it may have improved the patients care through imaging of the bladder with a better resolution of the tissue planes, there is still need to perform an invasive procedure to have a sample for pathological examination.

Received: January 4, 2022
Accepted: March 3, 2022
Published: March 17, 2022

Sensitive and precise detection of chemical changes in biomolecules due to development of cancers is possible using vibrational spectroscopy methods, namely infrared (IR) absorption,[9] Raman spectroscopy,[10−12] and surface-enhanced Raman scattering (SERS) spectroscopy.[13−16] It has been previously shown that both of these methods can be used to discriminate between the cancerous and normal tissues or cells of various cancers, like brain,[17−20] breast,[21−24] or others.[25−28] Similarly, we have showed that SERS and attenuated total reflectance Fourier-transform infrared (ATR-FTIR) methods can be used to detect kidney cancer through the analysis of the extracellular fluid.[29,30] Nowadays, a lot of research has been focused to nondirect cancer detection through "liquid biopsies" since this method can be potentially noninvasive.[31−33] A number of vibrational spectroscopy studies have been performed regarding bladder cancer as well.[34−41] It has been shown that FTIR spectroscopy can be used not only to distinguish cancerous and normal bladder tissues[34,35] but also to detect bladder cancer from bladder washings.[36] Raman spectroscopy possesses several advantages comparing with other spectroscopy methods, such as (i) negligible interference from water, (ii) rich vibrational information on bonding and interactions of molecular groups, (iii) narrow vibrational bands, and (iv) resonance and surface enhancement possibilities. The SERS technique overcomes the low inherent sensitivity of ordinary Raman spectroscopy. Several groups have demonstrated the promising advantages of the SERS approach in analysis of bladder cancer.[37−52] The first attempts to employ SERS spectroscopy for the analysis of the cultured bladder cancer cells are described by Jin et al.[37] in 2015. Following studies have shown that in vivo imaging of the bladder tissue can be performed using SERS nanotags[38] or that the noninvasive and muscle-invasive bladder cancer cells can be determined from liquid biopsies.[39] Importance of development of new highly effective SERS substrates for analysis of bladder cancer cells was well-recognized.[40,42] Thus, highly ordered silver nanopore and nanocap arrays were fabricated by using porous layers of anodic alumina membranes.[42] Recently, Chuang et al.[40] demonstrated the advantages of hollow Au_xCu_{1-x} alloy nanoshells for SERS detection of bladder cancer cells. Progress in SERS-based discrimination of various cancer cell types including bladder cancer cells was achieved by combining antibody-conjugated magnetic beads and antigen-targeting SERS nanotags.[45] To improve the detection precision, an internal-reference based ratio-metric SERS assay method[41] and dual-mode Au-nanoprobe technique based on determination of telomerase activity in cell extracts and urine of patients by combining SERS and calorimetry measurements[46] were developed. The potential of SERS spectroscopy for discrimination of high-grade and low-grade bladder cancer cells was demonstrated.[47−49] The possibility to predict the bladder cancer grade by SERS analysis of urine supernatant and sediment was proposed.[47] Recently, a new elegant NIR-SERS platform based on modified Au−Ag nanohollows was developed for effective discrimination of high-grade and low-grade bladder cancer cells.[48]

In this work, we demonstrated that a label-free SERS spectroscopy approach, in comparison with other approaches, can be applied much more easily while still granting sensitive chemical analysis. The analysis of extracellular fluid of bladder tissue and the tissue itself was performed. We have employed near-infrared (1064 nm) excitation wavelength ensuring nonresonant and fluorescence-free SERS spectra of biosamples. It was demonstrated that combination of near-infrared excitation and citrate-reduced Ag nanoparticles as a substrates increases repeatability of SERS spectra of biofluids.[53] If a precise label-free SERS method would be developed it could be further improved to benefit the clinical diagnosis. By employing optical fiber probes SERS method is already being proposed as a sensitive method allowing on site analysis.[54] Thus, if coupled with endoscopic analysis, fiber probes covered with SERS active nanoparticles could be used to enhance the sensitivity and minimize the invasiveness of the tumor detection.

2. MATERIALS AND METHODS

2.1. Sample Collection. Spectral studies of the bladder tissues were approved by the Vilnius Regional Biomedical Research Ethics Committee (Document No. 2019/12-1178-665). The samples of the bladder tissues for SERS spectroscopic studies were obtained between December 2019 and March 2020 in the Urology Center of the Vilnius University Hospital Santaros Clinics when performing transurethral resection of urinary bladder (TURB) or radical cystectomy (RC). Patients were eligible if they had a clinical or radiological suspicion of bladder cancer and they required any of the procedures mentioned (TURB, RC) according to the latest guidelines for bladder cancer of the European Association of Urology. All patients gave an informed consent. Ineligibility criteria were refusal to participate in the study, positive urine culture, and untreated coagulopathy.

At the beginning of the TURB procedure, before cutting the tumor, a single sample of healthy-looking bladder tissue was obtained for the spectral studies. After the TURB procedure, a single sample of cancer-suspicious tissue was obtained for the spectral studies. Malignancy was confirmed pathologically by examining the remaining resected tissue. When performing RC, samples of healthy and malignant tissue were obtained after the procedure. Immediately after surgery, bladder tissue samples were submitted for histological and spectroscopic analysis. Thus, every set of samples gathered for the spectroscopic analysis contained the cancerous or cystitis-affected tissue and the healthy-looking tissue, which was collected from the bladder of the same patient. The latter tissue type for the purpose of convenience is called normal tissue in the manuscript. The true nature of the tissue that was considered as healthy-looking was proved by the results of histological examination.

2.2. Sample Preparation. Samples for the SERS analysis of the whole tissue were prepared as follows. The small part of the bulk tissue was cut with a clean scalpel blade. The resected bladder cancer tissues were rather small due to the limitations of the surgery (the resection procedure). Therefore, on average, the analyzed tissue samples were around 1.5−2 mm in diameter. Subsequently, the cut of tissue was placed with the cut side up, and a small amount of the concentrated colloidal solution was deposited on top and dried. The SERS spectra were then collected directly from the surface of the tissue.

Samples of extracellular fluid of the normal, cystitis-affected, and cancerous bladder tissues analyzed in this work were prepared in the following manner. A small part of the bladder tissue was sliced off the bulk tissue and smeared (pressing the cut side) across the aluminum substrate, which was precleaned with methanol. The formed extracellular fluid layer was dried in an open environment at room temperature and used for further studies. Such a sample preparation procedure results in

https://doi.org/10.1021/acsomega.2c00058
ACS Omega 2022, 7, 10539−10549

creation of a thin film of extracellular fluid, which also includes single cells of the tissue. Since the samples of extracellular fluid were taken by stamping of the tissue under study on glass substrate, the stamp retains information about the morphology of the tissue. The cancerous areas of the tissue are located in the same places in the stamp, just with a much lower concentration of the cells. Before collecting the SERS spectra, a drop of colloidal solution was put on the top of dried extracellular fluid film.

To ensure reproducibility of the SERS data, the same procedure for the preparation of the samples and the colloidal solution was reproduced in a very thorough and careful manner in order to keep the experimental parameters always the same (or at least as similar as possible). Therefore, high reproducibility of the SERS spectra was achieved in this study. The volume of the colloidal solution added on top of the extracellular fluid or tissue sample for each measurement was always the same, 10 μL. Therefore, the incubation time of the AgNPs and the tissue or extracellular fluid layer samples was relatively constant. The samples were measured immediately after the nanoparticle solution drop was dried. Since small drops of liquid were used, the drying process took around 30 s.

2.3. Measurement Equipment. The UV−vis electronic absorption spectra of silver nanoparticles were recorded using a two-channel UV−vis−NIR spectrophotometer Lambda 1050 (PerkinElmer, USA) equipped with two light sources, deuterium and halogen lamps. Spectra were collected in a wavelength range of 250 to 1100 nm and a resolution of 5 nm were selected.

The Raman scattering and the SERS spectra were collected using Fourier Transform (FT-Raman) MultiRAM spectrometer (Bruker GmbH, Germany). The samples were irradiated using 1064 nm wavelength Nd:YAG laser. Spectra collection was done in 180-deg geometry. Gold plated hyperbolic 90-deg angle mirror objective coupled with a CCD camera was used. The focal length of the objective was 33 mm and the diameter of the focused laser beam was 100 μm (an average intensity at the sample of 955 W/cm^2 at 100 mW of laser power). A liquid nitrogen cooled Ge detector was used to collect the scattered light. All spectra were collected in the wavenumber range of 100−3600 cm^{-1} with a resolution of 4 cm^{-1}. A Blackman−Harris 3 term apodization function and a zero-filling factor of 2 were used for the Fourier transform. To avoid time-dependent changes in the biosample and increase repeatability of the measurements, the time required to prepare the sample with Ag nanoparticles and acquire the SERS spectrum was sufficiently short, no longer than 5 min.

The variability of the experimental and SERS spectra was calculated as follows. First, using the normalized experimental spectra, the averaged SERS spectrum was calculated for each class: cancer, normal, and cystitis. Second, using the spectral data, the standard deviation was calculated for each individual data point. Finally, the standard deviation was visualized together with the averaged spectra for each class.

2.4. Preparation and Characterization of the Colloidal Solution of Silver Nanoparticles. Silver nanoparticles were prepared in accordance to the procedure described by Lee and Meisel.[55] In short, 18 mg of silver nitrate ($AgNO_3$, 99%, Merck, Germany) was dissolved in 100 mL of distilled water. Next, an aqueous solution of $AgNO_3$ was heated to boiling temperature while stirring constantly. When the boiling point was reached, 2 mL of a 1% solution of trisodium citrate ($Na_3C_6H_5O_7$, 99%, Merck, Germany) was added, and the whole mixture was left heated for an additional hour while being stirred rapidly. After 1 h, the solution was cooled to a room temperature in an ice-bath. The synthesis procedure results in a grayish-green solution of silver nanoparticles. To increase the concentration of nanoparticles, the colloidal solution was centrifuged for 10 min at 6500 rpm. After that, 15 mL out of the initial 30 mL solution was removed as a supernatant. The left-over concentrated solution was used for the Raman scattering measurements.

Biological media may affect the stability of synthesized Ag nanoparticles.[56,57] Based on SERS measurements, we found that the nanoparticles remained stable for more than 2 h. This might be related to the fact that the samples of extracellular fluid of bladder tissue and colloidal solution were dried. Also, the whole process of sample preparation and SERS measurement was rather short, no longer than 5 min. Recently, Valenti and Giacomell[57] have demonstrated the stability of citrate-capped Ag nanoparticles against dissolution in biologically relevant conditions. The stability of silver nanoparticles capped with different agents (including citrate), in various conditions of biological media (different pH levels, electrolyte concentration, buffers) was investigated by MacCuspie.[56] It was found that the performance of the citrate-capped Ag nanoparticles can be observed up to 5 h or more.

3. RESULTS AND DISCUSSION

3.1. Characterization of Silver Nanoparticles. Silver nanoparticles were characterized by UV−vis spectroscopy and transmission electron microscopy (TEM) analysis (Figure S1). Only one broad band centered at 450 nm was observed in the UV−vis spectrum. Integrated intensity of this band was found to increase by a factor of 1.6 after centrifugation (6500 rpm) indicating an increase in concentration of Ag nanoparticles. Based on analysis of TEM image, the average diameter of spherical nanoparticles was found to be about 80 nm. The size distribution of synthesized Ag nanoparticles is shown in Figure S2. The suitability of Ag nanoparticles for SERS studies was tested by using uric acid as an adsorbate (Figure S3). The calculated analytical enhancement factor for centrifuged at 6500 rpm nanoparticles was found to be 8×10^4.

Before conduction of the experiments with biological samples, the SERS spectrum of the bare Ag nanoparticles was recorded (Figure 1). Such a spectrum is needed in order to eliminate the bands present from adsorbed stabilizing species or impurities, which might seriously perturb the spectrum of samples under investigation.[13,58] The strong feature near 236 cm^{-1} dominates in the SERS spectrum. Similar intense band (232 cm^{-1}) was observed previously in SERS spectrum of citrate-reduced Ag nanoparticles.[59] This band was assigned to the stretching vibration of silver−oxygen bond. It should be noted that stretching vibration of Ag−Cl bond occurs in the similar wavenumber region.[60] A small amount from chloride salt impurities in chemical compounds used for preparation of Ag nanoparticles may contribute to the observed low-frequency band. In this work, chloride salts were not used for synthesis of Ag nanoparticles. Therefore, the stretching vibration of Ag−O bond was suggested as a major contribution for the low-frequency band at 236 cm^{-1} observed in this work. Thus, the low frequency spectral region is not useful for analysis of biological samples; however, the frequency region above 300 cm^{-1} does not contain any distinct spectral features and was explored for further SERS analysis.

https://doi.org/10.1021/acsomega.2c00058
ACS Omega 2022, 7, 10539−10549

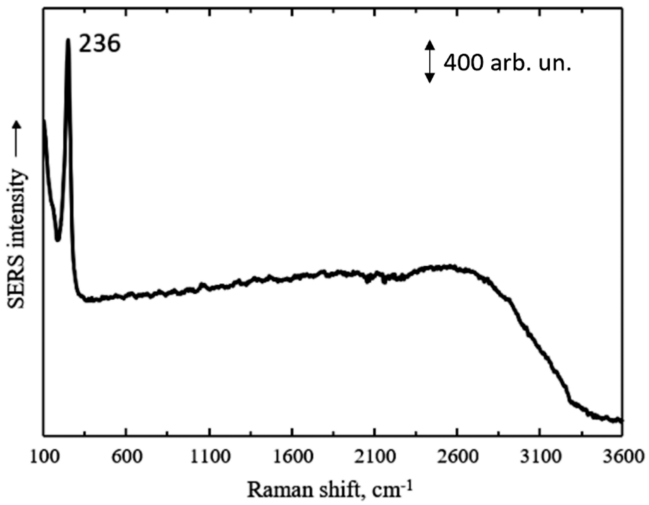

Figure 1. SERS spectrum of the centrifuged colloidal solution of silver nanoparticles used in this study. The excitation wavelength is 1064 nm.

3.2. Comparison of Raman and SERS spectra. Figure 2 compares Raman and SERS spectra of normal and cancerous

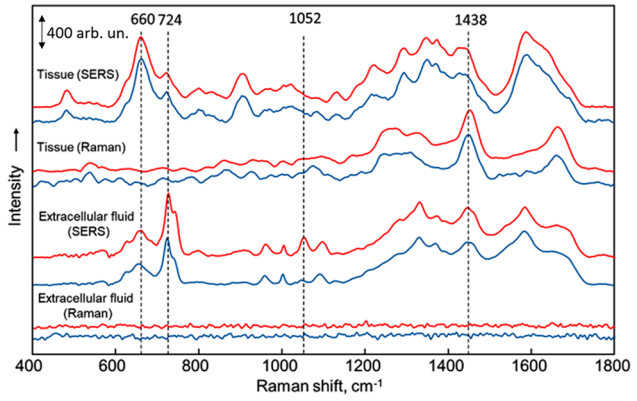

Figure 2. Comparison of conventional Raman and SERS spectra of normal (lower spectra, blue curve) and cancerous (upper spectra, red curve) bladder tissues and their extracellular fluids. Values of Raman shifts over broken bars denote the bands related with the strongest spectral changes. The excitation wavelength is 1064 nm.

bladder tissues and their extracellular fluid. One can see that ordinary Raman spectra differ considerably comparing with the SERS spectra from the same samples. Raman spectra from tissue samples exhibit strong bands related to CH_2 deformation vibration near 1438 cm^{-1}, the Amide-I stretching mode at 1660 cm^{-1}, and broad features in the range 1250−1350 cm^{-1} mainly due to the Amide-III vibrational mode.[61] In contrast, SERS spectra of tissue exhibit many intense bands in the lower frequency region. This is because SERS spectrum represent adsorbed species at the surface of Ag nanoparticles and operation of special surface selection rules.[58,62] In the case of extracellular fluids, no ordinary Raman spectra are observed; however, intense SERS spectra are acquired. As can be observed, conventional Raman scattering spectra do not provide clear information on the nature of the sample (normal or cancerous). Slight spectral differences can be observed in the Raman spectra of the tissue but these differences are extremely small, and any discrimination of the tissues would be complicated. Compared to that, spectral differences between normal and cancerous samples observed in the SERS spectra are much greater (especially in the case of extracellular fluid samples). Because of the intense spectra from extracellular fluids and strong response in the fingerprint spectral region of tissue samples, in the following we will discuss only the SERS studies.

3.3. SERS Spectroscopy of Bladder Tissue Samples. The total of 58 bladder tissue samples of 30 different patients (28 healthy, 25 cancer patients, and 5 patients affected by cystitis) were collected and studied in this work. The histological examination was performed for all the collected samples. The results of histological analysis of the bladder tissues used in this study are presented in Table 1. Cancers were classified by TNM (tumor node metastasis), a globally recognized standard for classification the extent of spread of cancer.

Table 1. Results of Histological Analysis of Bladder Tissues Used in the Study

histological type	TNM[a]	differentiation grade	number of patients
urothelial carcinoma	pTa	low-grade	9
urothelial carcinoma	pTa	high-grade	8
urothelial carcinoma	pT1	high-grade	3
urothelial carcinoma	pT2a	high-grade	2
urothelial carcinoma	pT2b	high-grade	1
urothelial carcinoma	pT3a	high-grade	2
nonspecific cystitis	–	–	5

[a]Abbreviation: TNM, tumor node metastasis.

For determination of the spectral differences between healthy, cancerous, and cystitis-affected bladder tissues, SERS spectra were recorded. The spectra were collected at five different points for each of the bladder samples (tissues and their extracellular fluid layers) in order to take into account possible differences of the spectra at different measuring points. The averaged SERS spectra of bladder tissues are presented in Figure 3. The spectra were normalized by

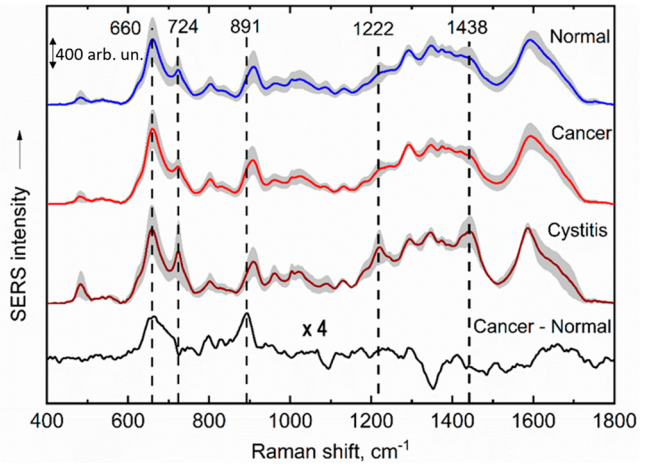

Figure 3. Averaged SERS spectra of cystitis-affected, cancerous and normal bladder tissue samples and the difference spectrum with a magnified intensity (×4) between the averaged spectra of cancerous and normal tissues. The gray areas in the spectra represent the standard deviation of the intensity. The excitation wavelength is 1064 nm.

https://doi.org/10.1021/acsomega.2c00058
ACS Omega 2022, 7, 10539−10549

applying vector normalization and were shifted along the SERS intensity axis for clarity. Gray areas indicate the standard deviation of the intensity of the SERS spectral bands. These changes may be reasoned by the concentration variations due to nonuniform distribution of structural molecules. The distribution of cancer relevant molecules in the human body depends on physiology, lifestyle, physical activity, food intake, medication, illnesses, and other factors. Furthermore, in the case of cancer, the concentration of such molecules in the tissue may vary with different type of the tumor, its stage, and morphological changes in the cancer cells. It is also important to note that during the surgery the exact borderline between normal and cancerous tissues is invisible. Therefore, cancerous cells can be detected in a sample of a healthy tissue sample and vice versa.

Analysis of the averaged SERS spectra of healthy and cancerous bladder tissue revealed that no significant spectral differences can be determined between them. To enhance small spectral deviations between the studied samples, we have constructed the difference spectrum; such an approach was previously used for detailed Raman/SERS analysis of bladder cancer.[11,47,50,51] The difference spectrum between the spectra of cancerous and normal tissues showed two spectral bands of interest (Figure 3). These are located at 660 and 891 cm^{-1}. Also, by comparison of these spectra with the SERS spectra of tissues affected by cystitis, three SERS spectral bands that are absent or have low intensity in the spectra of normal and cancerous tissues were identified. These bands are located at 724, 1222, and 1438 cm^{-1}. In order to explain the observed differences in the SERS spectra of urinary bladder tissues, a tentative assignment of the SERS bands was performed in accordance with the literature.[13,44,61−73] It can be stated that the main spectral differences may be related to the SERS spectral bands of Amide III (1222 cm^{-1}), adenine (724 cm^{-1}), cysteine (660 and 891 cm^{-1}), and proteins (1438 cm^{-1}). In addition, the 1438 cm^{-1} band may have some contribution from oxygenated guanosine ring stretching vibrations.[72] It should be noted that all of the spectral bands are directly related to the constituents of the analyzed samples and not the molecules in the composition of the colloidal solution itself. No distinct spectral bands in the discussed spectral region were observed in the SERS spectrum of the colloidal solution (see Figure 1).

3.4. SERS Spectroscopy of Extracellular Fluid. The sample smearing technique was chosen in this work, since it was already used in our previous studies where we have shown that extracellular fluid samples also contain single tissue cells.[29,30] In these studies, we have tested the reproducibility of such samples and have noticed that only minor changes in the intensity of the spectral bands are observed. To average out the small spectral differences which result from the small variation of the sample composition or thickness, the SERS spectra of extracellular fluid were also collected at five randomly chosen points of every sample. The two different measurement points were at least 1 mm apart. It should also be noted that the diameter of the focused laser spot in our experiments was 100 μm what is a relatively large area if compared to Raman microscopy measurements. Collection of the SERS signal from such area could be regarded as an averaging of the spectral information since in Raman microscopy the diameter of the area of measurement is only few micrometers. To represent the reproducibility of a typical sample, the SERS spectra collected at five randomly selected points of the extracellular fluid of normal bladder tissue is presented in the Figure 4. As can be observed, only slight differences in intensity result from the point of measurement.

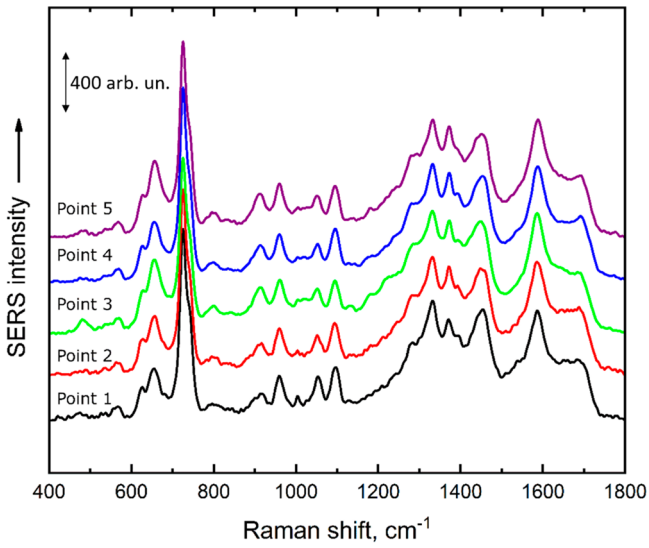

Figure 4. SERS spectra of extracellular fluid of normal bladder tissue collected at five randomly selected points of the sample. The excitation wavelength is 1064 nm.

An important matter is the spectral variance source. Figure 5 compares averaged intrasample and interpatient SERS spectra.

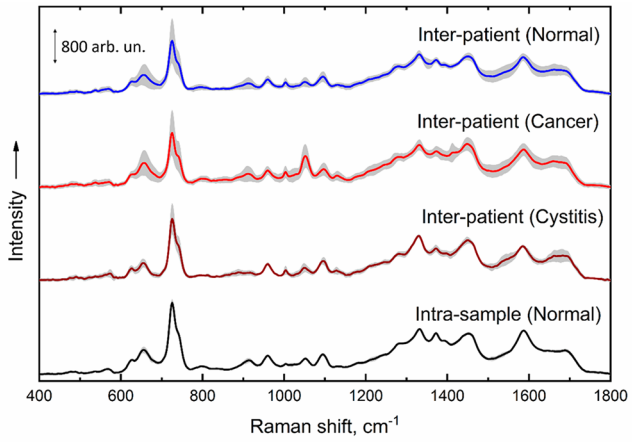

Figure 5. Comparison of averaged intrasample and interpatient SERS spectra of extracellular fluid of normal, cancer, and cystitis-affected samples. The gray areas in the spectra represent the standard deviation of the intensity. The excitation wavelength is 1064 nm. Five experimental spectra were averaged.

One can see that the intrasample variance is quite small in comparison to the interpatient spectra. This shows that the variance comes from the differences in the tissues of the patients. Such differences are a result of diseases and their progression in case of spectra of the cancerous or cystitis-affected samples and most probably the different lifestyles (food, metabolism, etc.) in the case of normal samples. The SERS spectra of extracellular fluid of healthy, tumor, and cystitis-affected tissues containing single cells are presented in Figure 6. It is notable that the standard deviation of the intensity of the vibrational bands (visualized by gray area) in

https://doi.org/10.1021/acsomega.2c00058
ACS Omega 2022, 7, 10539−10549

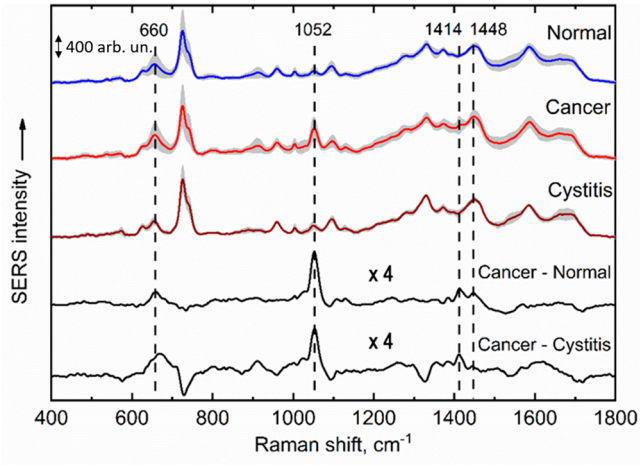

Figure 6. Averaged SERS spectra of the extracellular fluid of cystitis-affected, cancerous, and normal bladder tissues and the difference spectra with a magnified intensity (×4) between the averaged extracellular fluid of cancerous and normal and cancerous and cystitis-affected tissues. The gray areas in the spectra represent the standard deviation of the intensity. The excitation wavelength is 1064 nm.

these spectra may be attributed not only to the individual changes due to different lifestyle of each patient but also to the peculiarities of the sample preparation—the uneven surface of the extracellular fluid layers. This is because the intensity of the conventional and surface enhanced Raman scattering signals depends on the thickness of the test specimen (the number of the molecules contributing to the Raman signal). A very thin layer of an extracellular fluid with single cells results in the sufficiently strong SERS signal, while the SERS spectrum of the thick layer may resemble the Raman spectrum of the whole tissue.

The main spectral differences that allow the discrimination of the healthy and cancerous tissues can be observed in the SERS spectra of extracellular fluid presented in Figure 6. These vibrational spectral bands are located at 1052 and 1414 cm^{-1}, respectively. The SERS band of the extracellular fluid of cancerous bladder tissue at 1052 cm^{-1} is rather intense, while the band at 1414 cm^{-1} is less intense in the spectra of healthy and cystitis-affected tissues. Some SERS spectra of healthy tissue do not contain these bands at all.

Spectral alterations are more clearly visible in the SERS-difference spectrum (Figure 6) constructed from averaged cancerous and normal and cancerous and cystitis affected bladder spectra. The positive-going features in this spectrum are related with an additional or intensified bands characteristic for cancerous samples. Thus, an intense and sharp positive-going feature is visible at 1052 cm^{-1}, while two lower intensity bands appear near 1414 and 660 cm^{-1}. It should be noted that intensification of the latter band is not clearly visible from the averaged SERS spectra of the extracellular fluid of the cancerous bladder tissue. In order to highlight the spectral differences and variability of the spectral marker bands, the positions of the marker bands, the mean intensity, and the standard deviation values observed in the SERS spectra of bladder tissues (Figure 3) and extracellular fluids (Figure 6) are listed in Table 2.

3.5. SERS Marker Bands of Bladder Cancer/Cystitis.

Let us define the origin of the bands, characteristic to cancerous samples (Table 3). SERS spectra of selected biomolecules which could contribute to the observed spectra of bladder samples obtained at 1064 nm excitation wavelength are presented in Figure 7. One can see that tyrosine residues from proteins, cysteine, ATP, thymine ring, guanine ring, and lactic acid may contribute to 1052 cm^{-1} band. In the case of Tyr and Thymine, this is a relatively low intensity feature compared with other modes of these compounds. However, in the case of lactic acid molecules, this is the dominant and characteristic vibrational mode. Cysteine molecules may also contribute to the observed spectra due to exhibition of broad and intense feature near 660 cm^{-1} associated to C−S stretching vibration in addition to the 1052 cm^{-1} band. Thus, based on examination of presented SERS spectra of selected compounds and literature data analysis we suggest that the major contribution for the band located at 1052 cm^{-1} comes from the ν(C−O), ν(C−N), and ν(C−C) stretching vibrations of lactic acid[44,60−69] and/or cysteine[70] molecules. The increased intensity of this band in the cancerous tissue can be also explained by the increased amount of the cysteine, since such compound is related to the development of cancer. More precisely, a correlation between the cancer growth and the availability of cysteine was shown to be especially strong in bladder cancer.[74] Thus, the uptake of cysteine molecules is seen to be increased in the cancerous tissue.[75]

The vibrational band in the SERS spectra of the extracellular fluid of the bladder cancer tissues, observed at 1414 cm^{-1}, was found to be associated with stretching vibrations of protein, DNA, lipids, and lactic acid molecules (Figure 7). SERS-difference spectrum suggests the presence of two positive-going features in this spectral region at 1414 and 1448 cm^{-1} (Figure 6). Intense bands in this spectral region are characteristic for lipid molecules due to scissoring bending vibration of methylene groups.[67] Lipids perform the function of cellular energy storage and are involved in signal transduction, cell proliferation, and growth processes. Since more energy is used during the uncontrolled division and

Table 2. Mean Values and the Standard Deviation of the Main Spectral Bands Observed in the SERS Spectra of Bladder Tissue and Extracellular Fluid

sample	wavenumber, cm^{-1}	I_{Normal}, au	I_{Cancer}, au	$I_{Cystitis}$, au
tissue	660	1.26 ± 0.42	1.38 ± 0.35	1.20 ± 0.40
	724	0.68 ± 0.28	0.69 ± 0.17	0.85 ± 0.49
	1222	0.62 ± 0.20	0.64 ± 0.14	0.92 ± 0.27
	1438	0.91 ± 0.20	0.90 ± 0.15	1.16 ± 0.23
extracellular fluid	660	0.58 ± 0.36	0.68 ± 0.38	0.50 ± 0.13
	1052	0.37 ± 0.17	0.89 ± 0.39	0.39 ± 0.16
	1414	0.86 ± 0.10	0.99 ± 0.26	0.83 ± 0.11
	1448	1.08 ± 0.07	1.20 ± 0.14	1.20 ± 0.09

https://doi.org/10.1021/acsomega.2c00058
ACS Omega 2022, 7, 10539−10549

Table 3. SERS Marker Bands of Bladder Cancer/Cystitis Based on Analysis of Tissue and Extracellular Fluid Samples

wavenumber, cm^{-1}	vibrational mode	molecular group	comments
724	A ring breathing	adenine ring in DNA	tissue; possible marker band of cystitis
1222	Amide-III	amide group in proteins	tissue; possible marker band of cystitis
1438	scissoring CH_2; W6; 8-oxo-dG ring stretching	methylene groups in proteins and lipids; tryptophan residue in proteins; 8-oxo-deoxyguanosine ring of DNA	tissue; possible marker band of cystitis
660	G ring breathing; C−S stretching	guanine ring in DNA; cysteine	extracellular fluid; marker band of cancer
1052	C−O, C−N, and C−C stretching	lactic acid; cysteine	extracellular fluid; best marker band of cancer
1414/1448	scissoring CH_2; W6; 8-oxo-dG ring stretching	methylene groups in proteins and lipids; tryptophan residue in proteins; 8-oxo-deoxyguanosine ring of DNA	extracellular fluid; marker band of cancer

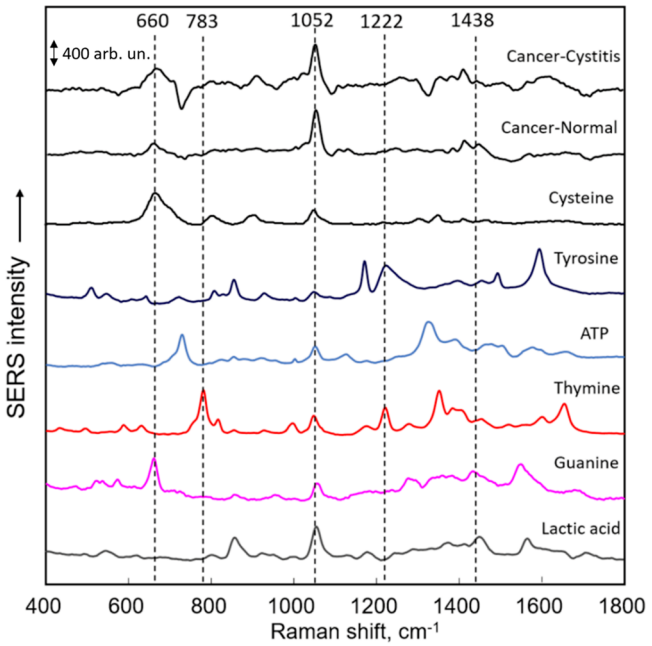

Figure 7. Difference spectra of extracellular fluid between the cancerous and cystitis affected, and cancerous and normal bladder tissues. The SERS spectra of different biomolecule solutions (1 mM) are also presented for comparison. The excitation wavelength is 1064 nm.

growth of cancer cells, lipid metabolism is disrupted in tumor cells.[76] The altered metabolism of these molecules may lead to different lipid concentrations in healthy and cancer cells. These changes depend on the type and stage of the cancer and its aggression. Changes in the intensity of these bands can be influenced by changes in the body's genetic material, which is typical for the cancer. It is known that structural mutations in DNA can be one of the causes of the formation of cancer cells. The increase of lactic acid concentration in cancerous tissue can be explained by the Warburg effect.[77] Adenosine triphosphate (ATP) molecules are the major source of energy in the cell. In healthy intact cells, most ATP is synthesized by oxidative phosphorylation in the presence of ADP (adenosine diphosphate) and phosphoric acid during oxidation−reduction reactions. However, cancer cells are characterized by a rapid process of glycolysis, the breakdown of glucose molecules into pyruvate molecules, and the formation of ATP molecules. Glycolysis (the anaerobic pathway for glucose metabolism), in terms of ATP synthesis, is not as efficient as oxidative phosphorylation. However, it produces metabolites that are useful for cell division and tumor growth, including lactic acid secreted during pyruvate fermentation.[78] Partial oxidation of DNA is also related with genomic mutations and development of cancer.[79] Kundu and Loppnow recently demonstrated that major oxidative damage of DNA associated with 8-oxodeoxyguanosine (8-oxo-dG) molecules can be reliably detected by ultraviolet resonance Raman spectroscopy.[72] The Raman marker band of 8-oxo-dG ring stretching vibration was found at 1449 cm^{-1}, which is close to our observed 1414/1448 cm^{-1} SERS bands.

The vibrational band observed in the SERS-difference spectrum at 660 cm^{-1} is most likely related to the breathing vibration of guanine rings in DNA or C−S stretching vibration of cysteine residues in proteins (Figure 7). This is again supported by the already mentioned role of the cysteine molecules in the proliferation of bladder cancer.

3.6. Principal Component Analysis (PCA) of the SERS Spectra. To evaluate the reliability and accuracy of the spectral features of the cystitis-affected bladder tissue, the principal components analysis (PCA) was performed using an algorithm built in the Origin Pro 9 software (OriginLab Corporation, Northampton, MA). However, due to the small data set, at this stage of the research, the PCA was conducted only in regard to the general clinical problem—discrimination between cancerous and normal bladder tissues. With a bigger data set, more in-depth analysis (for example, the classification of the SERS spectra in regard to the tumor grade or type)[47−49] could be carried out using a more sophisticated tools for statistical analysis. Such an analysis is planned in the future for this research when a larger data set will be gathered.

While performing the PCA, the spectral data were analyzed using the first five principal components. This number was chosen because together these components explain more than 97% of the variance in the case of spectral tissue data and more than 99% in the case of the spectral ECF data. Projections of the data in the space of various principal component combinations were produced and analyzed. However, the best results of the analysis, which are shown below, were observed using the first two principal components. The SERS spectra of the bladder tissues and the extracellular fluid were first analyzed in the whole spectral fingerprint region. The PCA analysis of the collected SERS spectra analysis performed on the whole spectral region has given unsatisfactory results in both cases (tissues and extracellular fluid) since the SERS spectra could not be separated into different groups (normal, cancerous, cystitis-affected). This may be reasoned by the intensity variation of the spectral bands of molecules which are not associated neither with cancerous nor cystitis-affected

https://doi.org/10.1021/acsomega.2c00058
ACS Omega 2022, 7, 10539−10549

tissues. The concentration of these molecules may differ due to other factors. Therefore, the change in the intensity of the spectral bands related to these molecules only introduce the unwanted variation (noise) which in result makes the PCA analysis more difficult.

Then the analysis was performed in the regions of the vibrational bands that can be used for identification the bladder tissue cancer and cystitis. The following regions of the SERS spectra, 700−750, 1190−1260, and 1400−1460 cm^{-1}, were selected for the bladder tissue spectra analysis. PCA performed in the spectral regions of potential markers bands revealed that the projections of the data of normal, cancerous, and cystitis-affected tissue spectra partly overlap in the plane of the principal components. No clear boundaries can be drawn between the groups of points corresponding to the spectra of different tissues. It can be assumed that variations in the intensity of the vibrational bands, which have been identified as spectral markers of cystitis-affected in bladder tissue studies, may be random and only depend on different patient physiology and other factors. For this reason, intensity changes of the respective bands cannot be attributed to groups of healthy, cancerous, or cystitis tissues that just exhibit features that are specific to these groups.

The spectral regions 600−750, 1020−1080, and 1390−1440 cm^{-1} were selected for the analysis of the SERS bands of the extracellular fluid with aim of tissue discrimination. The spectral bands observed at 660 (guanine, cysteine), 1052 (lactic acid, cysteine) and 1414 cm^{-1} (proteins, lipids, DNA, lactic acid) were identified as the possible spectral markers of cancer in the study of extracellular fluid layers of tissues. In the PCA diagrams of the spectral regions where 660 and 1414 cm^{-1} vibrational bands are observed, the points corresponding to the data of healthy and cancerous bladder tissues are widely distributed (Figures S4 and S5). Most of these points overlap. The dispersion of the points corresponding to the cystitis-affected tissues in the PCA diagram is also high, making it difficult to determine the possible area of their accumulation.

The PCA plot of the spectral region 1020−1080 cm^{-1} associated with the band that was assigned to lactic acid and cysteine vibrations shows a clearly distinguishable group of points corresponding to healthy patient data from all patients (Figure 8). Based on the small dispersion of these points, it can be assumed that the concentrations of the lactic acid and cysteine molecules, whose vibrations are assigned to the spectral band observed at 1052 cm^{-1} are similar in all of the healthy bladder tissues of different patients. In the case of the cancer tissue data, 4 of 21 points fall into the group of points corresponding to healthy tissue data. This may be influenced by the amount of healthy tissue removed with the tumor during the surgery, inaccuracies in the preparation of extracellular fluid layers, and other factors. The remaining 17 points are sufficiently distant from the group of points corresponding to healthy tissues to be considered as a separate group. These points are widely distributed in comparison to distribution of other points. A larger variance of the points can mean a greater difference between the elements that make up the data set. Such distribution can be explained by the fact that different malignant cancer cells may contain different amounts of lactic acid, or cysteine molecules, which are related to the proliferation of cancer and metastasis. In addition, larger tumors may have higher accumulations of these molecules. Thus, it can be argued that healthy and cancerous tissues contain different amount of such molecules, which is reflected

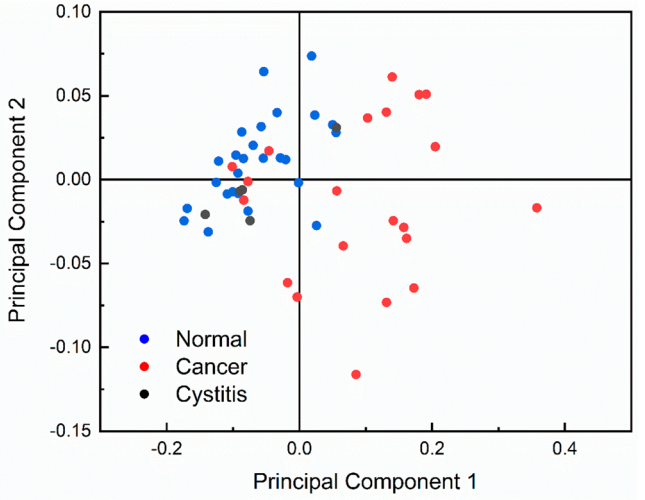

Figure 8. Principal component analysis (PCA) diagram of the 1020−1080 cm^{-1} wavenumber region of the SERS spectra of extracellular fluid of normal, cancerous, and cystitis-affected bladder tissue samples.

in the spectra. The points corresponding to the cystitis affected tissues in the PCA diagram overlap with the group of healthy tissue points. It can be stated that the changes in the intensity of the SERS spectra of the extracellular fluid layers of cystitis-affected tissues in the 1020−1080 cm^{-1} region are similar to the deviations observed in the extracellular fluid spectra of healthy tissues. Thus, an analysis of the principal components of the 1020−1080 cm^{-1} spectral data revealed that 81% of cancer tissue samples could be assigned to a separate group with greater data variance than healthy and cystitis-affected tissues. In comparison to the clinical standard this detection leads to the sensitivity of around 85% and specificity of around 97% remembering that distinguishing the cystitis affected tissue from the cancerous tissue is the sought-after result as well.

4. CONCLUSIONS

Three types of bladder tissues—normal, cancerous, and cystitis affected were examined. Significant spectral differences were observed in the SERS spectra of extracellular fluid of bladder tissues. The intensity of the spectral band, located at 1052 cm^{-1} and associated with lactic acid and/or cysteine, is the highest in the SERS spectra of the extracellular fluid of cancerous tissue, while it is less intense in the spectra of cystitis-affected tissue and the least intense in the spectra of normal tissue. This band can be considered as the best SERS spectral marker of the cancerous tissue. The PCA analysis in relation to the spectral marker has shown that the cancer tissue can indeed be distinguished from the normal and cystitis-affected tissues. With the limited data set used, the sensitivity and specificity of the methods were 85% and 97%, respectively. When the fluid is taken by the stamping technique, morphological information of the tissue persists in the dried fluid. However, the discrimination of the cystitis affected tissues from the normal and cancerous is more difficult since the intensity of the spectral bands related to internal vibrations of Amide III (1222 cm^{-1}), adenine (724 cm^{-1}), and proteins/lipids (1438 cm^{-1}) are more intense in the spectra of cystitis-affected tissues. Since the SERS spectroscopy is known to be very sensitive, the use of this method instead of the conventional Raman or the FTIR absorption spectroscopy

https://doi.org/10.1021/acsomega.2c00058
ACS Omega 2022, 7, 10539−10549

could increase the accuracy of detection of the cancerous tissue areas. The sensitivity and specificity of the method can be increased by using a larger data set, or implementing other colloidal solutions of nanoparticles could improve the spectroscopic analysis. Development of magneto-plasmonic nanoparticles[80−82] with increased efficiency for the SERS studies of the extracellular fluids is under way in our laboratory. To prove the NIR-SERS ability as a diagnostic tool for discrimination between cancerous and normal bladder cells via analysis of extracellular fluid, more studies with clinical cancer samples are required.

■ ASSOCIATED CONTENT

Supporting Information

The Supporting Information is available free of charge at https://pubs.acs.org/doi/10.1021/acsomega.2c00058.

UV−vis absorption spectra of Ag colloidal solution; TEM image of silver nanoparticles; size distribution of Ag nanoparticles; Raman and SERS spectra of uric acid; and principal component analysis diagrams of the 600−750 and 1390−1440 cm^{-1} wavenumber regions of the SERS spectra of the extracellular fluid of normal, cancerous, and cystitis affected bladder tissue samples (PDF)

■ AUTHOR INFORMATION

Corresponding Authors

Martynas Velička − *Institute of Chemical Physics, Faculty of Physics, Vilnius University, LT-10257 Vilnius, Lithuania*; Email: martynas.velicka@ff.vu.lt

Gediminas Niaura − *Institute of Chemical Physics, Faculty of Physics, Vilnius University, LT-10257 Vilnius, Lithuania; Department of Organic Chemistry, Center for Physical Sciences and Technology (FTMC), LT 10257 Vilnius, Lithuania*; orcid.org/0000-0002-2136-479X; Email: gediminas.niaura@ftmc.lt

Authors

Edvinas Zacharovas − *Institute of Chemical Physics, Faculty of Physics, Vilnius University, LT-10257 Vilnius, Lithuania*

Gediminas Platkevičius − *Clinic of Gastroenterology, Nephrourology, and Surgery, Institute of Clinical Medicine, Faculty of Medicine, Vilnius University, LT-03101 Vilnius, Lithuania*

Albertas Čekauskas − *Clinic of Gastroenterology, Nephrourology, and Surgery, Institute of Clinical Medicine, Faculty of Medicine, Vilnius University, LT-03101 Vilnius, Lithuania*

Arūnas Želvys − *Clinic of Gastroenterology, Nephrourology, and Surgery, Institute of Clinical Medicine, Faculty of Medicine, Vilnius University, LT-03101 Vilnius, Lithuania*

Valdas Šablinskas − *Institute of Chemical Physics, Faculty of Physics, Vilnius University, LT-10257 Vilnius, Lithuania*

Complete contact information is available at: https://pubs.acs.org/10.1021/acsomega.2c00058

Notes

The authors declare no competing financial interest.

■ ACKNOWLEDGMENTS

This project has received funding from the European Regional Development Fund (Project No. 01.2.2-LMT-K-718-03-0078) under a grant agreement with the Research Council of Lithuania (LMTLT). The authors gratefully acknowledge the Center of Spectroscopic Characterization of Materials and Electronic/Molecular Processes (SPECTROVERSUM Infrastructure) for use of Raman spectrometer.

■ REFERENCES

(1) Ferlay, J.; Soerjomataram, I.; Ervik, M.; Dikshit, R.; Eser, S.; Mathers, C.; Rebelo, M.; Parkin, D. M.; Forman, D.; Bray, F. Estimated cancer incidence, mortality and prevalence worldwide in 2012. 2013. 2015. *GLOBOCAN*, 2012, v1.0, accessed December 2020; http://globocan.iarc.fr/Default.asp.

(2) Sylvester, R. J.; Van Der Meijden, A. P. M.; Oosterlinck, W.; Witjes, J. A.; Bouffioux, C.; Denis, L.; Newling, D. W. W.; Kurth, K. Predicting recurrence and progression in individual patients with stage Ta T1 bladder cancer using EORTC risk tables: a combined analysis of 2596 patients from seven EORTC trials. *Eur. Urol.* **2006**, *49*, 466−477.

(3) Curtis, S. *Milken Institute 2016 Report on Bladder Cancer*; Milken Inst.: 2016.

(4) Mowatt, G.; N'Dow, J.; Vale, L.; Nabi, G.; Boachie, C.; Cook, J. A.; Fraser, C.; Griffiths, T. R. L. Photodynamic diagnosis of bladder cancer compared with white light cystoscopy: Systematic review and meta-analysis. *Int. J. Technol. Assess Health Care* **2011**, *27*, 3−10.

(5) Walsh, P. C.; Retik, A. B.; Vaughan, Jr., E. D.; Wein, A. J.; Kavoussi, L. R.; Novick, A. C.; Partin, A. W.; Peters, C. A. *Campbell's Urology*, 8th ed.; Elsevier: 2002.

(6) Moch, H.; Cubilla, A. L.; Humphrey, P. A.; Reuter, V. E.; Ulbright, T. M. The 2016 WHO Classification of Tumours of the Urinary System and Male Genital Organs-Part A: Renal, Penile, and Testicular Tumours. *Eur. Urol.* **2016**, *70*, 93−105.

(7) Birkhäuser, F. D.; Studer, U. E.; Froehlich, J. M.; Triantafyllou, M.; Bains, L. J.; Petralia, G.; Vermathen, P.; Fleischmann, M.; Thoeny, H. C. Combined ultrasmall superparamagnetic particles of iron oxide-enhanced and diffusion-weighted magnetic resonance imaging facilitates detection of metastases in normal-sized pelvic lymph nodes of patients with bladder and prostate cancer. *Eur. Urol.* **2013**, *64*, 953−960.

(8) Panebianco, V.; Narumi, Y.; Altun, E.; Bochner, B. H.; Efstathiou, J. A.; Hafeez, S.; Huddart, R.; Kennish, S.; Lerner, S.; Montironi, R.; Muglia, V. F.; Salomon, G.; Thomas, S.; Vargas, H. A.; Witjes, J. A.; Takeuchi, M.; Barentsz, J.; Catto, J. W. F. Multiparametric Magnetic Resonance Imaging for Bladder Cancer: Development of VI-RADS (Vesical Imaging-Reporting And Data System). *Eur. Urol.* **2018**, *74*, 294−306.

(9) Su, K. A.; Lee, W. L. Fourier transform infrared spectroscopy as a cancer screening and diagnostic tool: A review and prospects. *Cancers* **2020**, *12*, 115.

(10) Kanmalar, M.; Abdul Sani, S. F.; Kamri, N. I. N. B.; Said, N. A. B. M.; Jamil, A. H. B. A.; Kuppusamy, S.; Mun, K. S.; Bradley, D. A. Raman spectroscopy biochemical characterization of bladder cancer cisplatin resistance regulated by FDFT1: a review. *Cell. Mol. Biol. Lett.* **2022**, *27*, 9.

(11) Chen, H.; Li, X.; Broderick, N.; Liu, Y.; Zhou, Y.; Han, J.; Xu, W. Identification and characterization of bladder cancer by low-resolution fiber-optic Raman spectroscopy. *J. Biophotonics* **2018**, *11*, e201800016.

(12) Kong, K.; Kendall, C.; Stone, N.; Notingher. Raman spectroscopy for medical diagnostics –From in-vitro biofluid assays to in-vivo cancer detection. *Adv. Drug. Delivery Rev.* **2015**, *89*, 121−134.

(13) Bonifacio, A.; Cervo, S.; Sergo, V. Label-free surface-enhanced Raman spectroscopy of biofluids: fundamental aspects and diagnostic applications. *Anal. Bioanal. Chem.* **2015**, *407*, 8265−8277.

(14) Pilot, R.; Signorini, R.; Durante, C.; Orian, L.; Bhamidipati, M.; Fabris, L. A review on surface-enhanced Raman scattering. *Biosensors* **2019**, *9*, 57.

(15) Pyrak, E.; Krajczewski, J.; Kowalik, A.; Kudelski, A.; Jaworska, A. Surface enhanced Raman spectroscopy for DNA biosensors − How far are we? *Molecules* **2019**, *24*, 4423.
(16) Jaworska, A.; Malek, K.; Kudelski, A. Intracellular pH − Advantages and pitfalls of surface-enhanced Raman scattering and fluorescence microscopy − A review. *Spectrochim. Acta, Part A* **2021**, *251*, 119410.
(17) Aydin, O.; Altas, M.; Kahraman, M.; Bayrak, O. F.; Culha, M. Differentiation of healthy brain tissue and tumors using surface-enhanced Raman scattering. *Appl. Spectrosc.* **2009**, *63*, 1095−1100.
(18) Karabeber, H.; Huang, R.; Iacono, P.; Samii, J. M.; Pitter, K.; Holland, E. C.; Kircher, M. F. Guiding Brain Tumor Resection Using Surface-Enhanced Raman Scattering Nanoparticles and a Hand-Held Raman Scanner. *ACS Nano* **2014**, *8*, 9755−9766.
(19) Butler, H. J.; Brennan, P. M.; Cameron, J. M.; Finlayson, D.; Hegarty, M. G.; Jenkinson, M. D.; Palmer, D. S.; Smith, B. R.; Baker, M. J. Development of high-throughput ATR-FTIR technology for rapid triage of brain cancer. *Nat. Commun.* **2019**, *10*, 4501.
(20) Kowalska, A. A.; Berus, S.; Szleszkowski, L.; Kamińska, A.; Kmiecik, A.; Ratajczak-Wielgomas, K.; Jurek, T.; Zadka, Ł. Brain tumor homogenates analysed by surface-enhanced Raman spectroscopy: Discrimination among healthy and cancer cells. *Spectrochim. Acta, Part A* **2020**, *231*, 117769.
(21) Ali, M. H. M.; Rakib, F.; Al-Saad, K.; Al-Saady, R.; Goormaghtigh, E. An Innovative Platform Merging Elemental Analysis and Ftir Imaging for Breast Tissue Analysis. *Sci. Rep.* **2019**, *9*, 9854.
(22) Shen, L.; Du, Y.; Wei, N.; Li, Q.; Li, S.; Sun, T.; Xu, S.; Wang, H.; Man, X.; Han, B. SERS studies on normal epithelial and cancer cells derived from clinical breast cancer specimens. *Spectrochim. Acta, Part A* **2020**, *237*, 118364.
(23) Moisoiu, V.; Socaciu, A.; Stefancu, A.; Iancu, S. D.; Boros, I.; Alecsa, C. D.; Rachieriu, C.; Chiorean, A. R.; Eniu, D.; Leopold, N.; Socaciu, C.; Eniu, D. T. Breast cancer diagnosis by surface-enhanced Raman scattering of urine. *Appl. Sci.* **2019**, *9*, 806.
(24) Pramanik, A.; Mayer, J.; Patibandla, S.; Gates, K.; Gao, Y.; Davis, D.; Seshadri, R.; Ray, P. C. Mixed-dimensional heterostructure material-based SERS for trace level identification of breast cancer-derived exosomes. *ACS Omega* **2020**, *5*, 16602−16611.
(25) Su, K.-Y.; Lee, W.-L. Fourier Transform Infrared Spectroscopy as a Cancer Screening and Diagnostic Tool: A Review and Prospect. *Cancers* **2020**, *12*, 115.
(26) Guerrini, L.; Alvarez-Puebla, R. A. Surface-Enhanced Raman Spectroscopy in Cancer Diagnosis, Prognosis and Monitoring. *Cancers* **2019**, *11*, 748.
(27) Niciński, K.; Krajczewski, J.; Kudelski, A.; Witkowska, E.; Trzcińska-Danielewicz, J.; Girstun, A.; Kamińska, A. Detection of circulating tumor cells in blood by shell-isolated nanoparticle-enhanced Raman spectroscopy (SHINERS) in microfluidic device. *Sci. Rep.* **2019**, *9*, 9267.
(28) Bizzarri, A. R.; Cannistraro, S. Toward cancer diagnostics of the tumor suppressor p53 by surface enhanced Raman spectroscopy. *Sensors* **2020**, *20*, 7153.
(29) Pucetaite, M.; Velicka, M.; Urboniene, V.; Ceponkus, J.; Bandzeviciute, R.; Jankevicius, F.; Zelvys, A.; Sablinskas, V.; Steiner, G. Rapid intra-operative diagnosis of kidney cancer by attenuated total reflection infrared spectroscopy of tissue smears. *J. Biophotonics* **2018**, *11*, e201700260.
(30) Velicka, M.; Pucetaite, M.; Urboniene, V.; Ceponkus, J.; Jankevicius, F.; Sablinskas, V. Detection of cancerous kidney tissue by means of SERS spectroscopy of extracellular fluid. *J. Raman Spectrosc.* **2017**, *48*, 1744−1754.
(31) Zhang, Y.; Mi, X.; Tan, X.; Xiang, R. Recent Progress on Liquid Biopsy Analysis using Surface-Enhanced Raman Spectroscopy. *Theranostics* **2019**, *9*, 491−525.
(32) Sitnikova, V. E.; Kotkova, M. A.; Nosenko, T. N.; Kotkova, T. N.; Martynova, D. M.; Uspenskaya, M. V. Breast cancer detection by ATR-FTIR spectroscopy of blood serum and multivariate data-analysis. *Talanta* **2020**, *214*, 120857.
(33) Moisoiu, V.; Iancu, S. D.; Stefancu, A.; Moisoiu, T.; Pardini, B.; Dragomir, M. P.; Crisan, N.; Avram, L.; Crisan, D.; Andras, I.; Fodor, D.; Leopold, L. F.; Socaciu, C.; Bálint, Z.; Tomuleasa, C.; Elec, F.; Leopold, N. SERS liquid biopsy: An emerging tool for medical diagnosis. *Colloids Surf., B* **2021**, *208*, 112064.
(34) Al-Muslet, N. A.; Ali, E. E. Spectroscopic analysis of bladder cancer tissues using Fourier transform infrared spectroscopy. *J. Appl. Spectrosc.* **2012**, *79*, 139−142.
(35) Witzke, K. E.; Großerueschkamp, F.; Jütte, H.; Horn, M.; Roghmann, F.; Von Landenberg, N.; Bracht, T.; Kallenbach-Thieltges, A.; Käfferlein, H.; Brüning, T.; Schork, K.; Eisenacher, M.; Marcus, K.; Noldus, J.; Tannapfel, A.; Sitek, B.; Gerwert, K. Integrated Fourier Transform Infrared Imaging and Proteomics for Identification of a Candidate Histochemical Biomarker in Bladder Cancer. *Am. J. Pathol.* **2019**, *189*, 619−631.
(36) Gok, S.; Aydin, A. Z.; Sural, Y. S.; Zorlu, F.; Bayol, U.; Severcan, F. Bladder cancer diagnosis from bladder wash by Fourier transform infrared spectroscopy as a novel test for tumor recurrence. *J. Biophotonics* **2016**, *9*, 967−975.
(37) Jin, D.; Chen, H.; Cao, M.; Yang, G.; Xue, W.; Huang, Y. SERS measurement of the bladder cancer cells with the nanoparticles. *Pak. J. Pharm. Sci.* **2015**, *28*, 1853−1856.
(38) Davis, R. M.; Kiss, B.; Trivedi, D. R.; Metzner, T. J.; Liao, J. C.; Gambhir, S. S. Surface-Enhanced Raman Scattering Nanoparticles for Multiplexed Imaging of Bladder Cancer Tissue Permeability and Molecular Phenotype. *ACS Nano* **2018**, *12*, 9669−9679.
(39) Chen, S.; Zhu, S.; Cui, X.; Xu, W.; Kong, C.; Zhang, Z.; Qian, W. Identifying non-muscle-invasive and muscle-invasive bladder cancer based on blood serum surface-enhanced Raman spectroscopy. *Biomed. Opt. Express* **2019**, *10*, 3533−3544.
(40) Chuang, Y.-T.; Cheng, T.-Y.; Kao, T.-L.; Liao, M.-Y. Hollow AuxCu1−x alloy nanoshells for surface-enhanced Raman-based tracking of bladder cancer cells followed by triggerable secretion removal. *ACS Appl. Nano Mater.* **2020**, *3*, 7888−7898.
(41) Liang, X.; Zhang, P.; Ma, M.; Yang, T.; Zhao, X.; Zhang, R.; Jing, M.; Song, R.; Wang, L.; Fan, J. Multiplex ratiometric gold nanoprobes based on surface-enhanced Raman scattering enable accurate molecular detection and imaging of bladder cancer. *Nano Research* **2021**, DOI: 10.1007/s12274-021-3902-1.
(42) Liu, Y.; Huang, L. Q.; Wang, J.; Tong, H. M.; Yang, L.; Zhao, L. H.; Zhang, W. W.; Wang, L.; Zhu, J. Fabrication of silver ordered nanoarrays SERS-active substrates and their applications in bladder cancer cells detection. *Spectrosc. Spectral Anal.* **2012**, *32*, 386−390.
(43) Pallaoro, A.; Mirsafavi, R. Y.; Culp, W. T. N.; Braun, G. B.; Meinhart, C. D.; Moskovits, M. Screening for canine transitional cell carcinoma (TCC) by SERS-based quantitative urine cytology. *Nanomedicine: NBM* **2018**, *14*, 1279−1287.
(44) Jin, D.; Wang, X. T.; Fu, B.; Li, T. H.; Chen, N.; Chen, Z. Y.; Chen, H. G.; Liu, S. P. Raman spectroscopy of luminal subtype and basal subtype muscle invasive bladder cancer. *Int. J. Clin. Exp. Med.* **2019**, *12*, 5447−5453.
(45) Zhang, W.; Jiang, L.; Diefenbach, R. J.; Campbell, D. H.; Walsh, B. J.; Packer, N. H.; Wang, Y. Enabling sensitive phenotypic profiling of cancer-derived small extracellular vesicles using surface-enhanced Raman spectroscopy nanotags. *ACS Sens.* **2020**, *5*, 764−771.
(46) Feng, E.; Zheng, T.; Tian, Y. Dual-mode Au nanoprobe based on surface enhancement Raman scattering and colorimetry for sensitive determination of telomerase activity both in cell extracts and in the urine of patients. *ACS Sens.* **2019**, *4*, 211−217.
(47) Hu, D.; Xu, X.; Zhao, Z.; Li, C.; Tian, Y.; Liu, Q.; Shao, B.; Chen, S.; Zhao, Y.; Li, L.; Bi, H.; Chen, A.; Fu, C.; Cui, X.; Zeng, Y. Detecting urine metabolites of bladder cancer by surface-enhanced Raman spectroscopy. *Spectrochim. Acta, Part A* **2021**, *247*, 119108.
(48) Yang, Y.-T.; Hsu, I.-L.; Cheng, T.-Y.; Wu, W.-J.; Lee, C.-W.; Li, T.-J.; Cheung, C. I.; Chin, Y.-C.; Chen, H.-C.; Chiu, Y.-C.; Huang, C.-C.; Liao, M.-Y. Off-resonance SERS nanoprobe-targeted screen of biomarkers for antigens recognition of bladder normal and aggressive cancer cells. *Anal. Chem.* **2019**, *91*, 8213−8220.

https://doi.org/10.1021/acsomega.2c00058
ACS Omega 2022, 7, 10539−10549

(49) Zhang, Y.; Lai, X.; Zeng, Q.; Li, L.; Lin, L.; Li, S.; Liu, Z.; Su, C.; Qi, M.; Guo, Z. Classifying low-grade and high-grade bladder cancer using label-free serum surface-enhanced Raman spectroscopy and support vector machine. *Laser Phys.* **2018**, *28*, 035603.
(50) Li, S.; Li, L.; Zeng, Q.; Zhang, Y.; Guo, Z.; Liu, Z.; Jin, M.; Su, C.; Lin, L.; Xu, J.; Liu, S. Characterization and noninvasive diagnosis of bladder cancer with serum surface enhanced Raman spectroscopy and genetic algorithms. *Sci. Rep.* **2015**, *5*, 9582.
(51) Chen, S.; Zhu, S.; Cui, X.; Xu, W.; Kong, C.; Zhang, Z.; Qian, W. Identifying non-muscle-invasive and muscle-invasive bladder cancer based on blood serum surface-enhanced Raman spectroscopy. *Biomed. Opt. Express* **2019**, *10*, 3533−3544.
(52) Davis, R. M.; Kiss, B.; Trivedi, D. R.; Metzner, T. J.; Liao, J. C.; Gambhir, S. S. Surface-enhanced Raman scattering nanoparticles for multiplexed imaging of bladder cancer tissue permeability and molecular phenotype. *ACS Nano* **2018**, *12*, 9669−9679.
(53) Bonifacio, A.; Dalla Marta, S.; Spizzo, R.; Cervo, S.; Steffan, A.; Colombatti, A.; Sergo, V. Surface-enhanced Raman spectroscopy of blood plasma and serum using Ag and Au nanoparticles: a systematic study. *Anal. Bioanal. Chem.* **2014**, *406*, 2355−2365.
(54) Cao, J.; Zhao, D.; Mao, Q. A highly reproducible and sensitive fiber SERS probe fabricated by direct synthesis of closely packed AgNPs on the silanized fiber taper. *Analyst* **2017**, *142*, 596−602.
(55) Lee, P. C.; Meisel, D. Adsorption and surface-enhanced Raman of dyes on silver and gold sols. *J. Phys. Chem.* **1982**, *86*, 3391−3395.
(56) MacCuspie, R. I. Colloidal stability of silver nanoparticles in biologically relevant conditions. *J. Nanopart. Res.* **2011**, *13*, 2893−2908.
(57) Valenti, L. E.; Giacomelli, C. E. Stability of silver nanoparticles: agglomeration and oxidation in biological relevant conditions. *J. Nanopart. Res.* **2017**, *19*, 156.
(58) Langer, J.; Jimenez De Aberasturi, D.; Aizpurua, J.; Alvarez-Puebla, R. A.; Auguié, B.; Baumberg, J. J.; Bazan, G. C.; Bell, S. E. J.; Boisen, A.; Brolo, A. G.; et al. Present and future of surface-enhanced Raman scattering. *ACS Nano* **2020**, *14*, 28−117.
(59) Munro, C. H.; Smith, W. E.; Garner, M.; Clarkson, J.; White, P. C. Characterization of the surface of a citrate-reduced colloid optimized for use as a substrate for surface-enhanced resonance Raman scattering. *Langmuir* **1995**, *11*, 3712−3720.
(60) Perales-Rondon, J. V.; Hernandez, S.; Martin-Yerga, S.; Fanjul-Bolado, P.; Heras, A.; Colina, A. Electrochemical surface oxidation enhanced Raman scattering. *Electrochim. Acta* **2018**, *282*, 377−383.
(61) Kocherbitov, V.; Latynis, J.; Misiūnas, A.; Barauskas, J.; Niaura, G. Hydration of lysozyme studied by Raman spectroscopy. *J. Phys. Chem. B* **2013**, *117*, 4981−4992.
(62) Matulaitienė, I.; Kuodis, Z.; Matijoška, A.; Eicher-Lorka, O.; Niaura, G. SERS of the positive charge bearing pyridinium ring terminated self-assembled monolayers: Structure and bonding spectral markers. *J. Phys. Chem. C* **2015**, *119*, 26481−26492.
(63) Mert, S.; Ozbek, E.; Otunctemur, A.; Culha, M. Kidney tumor staging using surface-enhanced Raman scattering. *J. Biomed. Optics* **2015**, *20* (4), 047002.
(64) Mert, S.; Culha, M. Surface-Enhanced Raman Scattering-Based Detection of Cancerous Renal Cells. *Appl. Spectrosc.* **2014**, *68*, 617−624.
(65) Zdaniauskienė, A.; Charkova, T.; Ignatjev, I.; Melvydas, V.; Garjonytė, R.; Matulaitienė, I.; Talaikis, M.; Niaura, G. Shell-isolated nanoparticle-enhanced Raman spectroscopy for characterization of living yeast cells. *Spectrochim. Acta, Part A* **2020**, *240*, 118560.
(66) Premasiri, W. R.; Lee, J. C.; Sauer-Budge, A.; Théberge, R.; Costello, C. E.; Ziegler, L. D. The biochemical origins of the surface-enhanced Raman spectra of bacteria: a metabolimics profiling by SERS. *Anal. Bioanal. Chem.* **2016**, *408*, 4631−4647.
(67) Czamara, K.; Majzner, K.; Pacia, M. Z.; Kochan, K.; Kaczor, A.; Baranska, M. Raman spectroscopy of lipids: a review. *J. Raman Spectrosc.* **2015**, *46*, 4−20.
(68) Szymanska-Chargot, M.; Chylinska, M.; Pieczywek, P. M.; Rösch, P.; Schmitt, M.; Popp, J.; Zdunek, A. Raman imaging changes in the polysaccharides distribution in the cell wall during apple fruit development and senescence. *Planta* **2016**, *243*, 935−945.
(69) Barrett, T. W. Laser Raman spectra of mono-, oligo- and polysaccharides in solution. *Spectrochim. Acta, Part A* **1981**, *37*, 233−239.
(70) Stewart, S.; Fredericks, P. M. Surface-enhanced Raman spectroscopy of peptides and proteins adsorbed on an electrochemically prepared silver surface. *Spectrochim. Acta, Part A* **1999**, *55* (1999), 1615−1640.
(71) Podstawka, E.; Niaura, G. Potential-dependent characterization of bombesin adsorbed states on roughened Ag, Au, and Cu electrode surfaces at physiological pH. *J. Phys. Chem. B* **2009**, *113*, 10974−10983.
(72) Kundu, L. M.; Loppnow, G. R. Direct detection of 8-oxo-deoxyguanosine using UV resonance Raman spectroscopy. *Photochem. Photobiol.* **2006**, *83*, 600−602.
(73) Yao, G.; Huang, Q. DFT and SERS Study of L-Cysteine Adsorption on the Surface of Gold Nanoparticles. *J. Phys. Chem. C* **2018**, *122*, 15241−15251.
(74) Combs, J. A.; DeNicola, G. M. The Non-Essential Amino Acid Cysteine Becomes Essential for Tumor Proliferation and Survival. *Cancers* **2019**, *11*, 678.
(75) Serpa, J. Cysteine as a Carbon Source, a Hot Spot in Cancer Cells Survival. *Front. Oncol.* **2020**, *10*, 947.
(76) Long, J.; Zhang, C.-J.; Zhu, N.; Du, K.; Yin, Y.-F.; Tian, X.; Liao, D.-F.; Qin, L. Lipid metabolism and carcinogenesis, cancer development. *Am. J. Cancer Res.* **2018**, *8*, 778−791.
(77) Warburg, O. On the Origin of Cancers Cells. *Science* **1956**, *123*, 309−314.
(78) Cheng, Y.; Yang, X.; Deng, X.; Zhang, X.; Li, P.; Tao, J.; Qin, C.; Wei, J.; Lu, Q. Metabolomics in bladder cancer: a systematic review. *Int. J. Clin. Exp. Med.* **2015**, *8*, 11052−11063.
(79) Schärer, O. D. Chemistry and biology of DNA repair. *Angew. Chem., Int. Ed. Engl.* **2003**, *42*, 2946−2974.
(80) Mosier-Boss, P. A. Review of SERS substrates for chemical sensing. *Nanomaterials* **2017**, *7*, 142.
(81) Wang, C.; Meloni, M. M.; Wu, X.; Zhuo, M.; He, T.; Wang, J.; Wang, C.; Dong, P. Magnetic plasmonic particles for SERS-based bacteria sensing: A review. *AIP Adv.* **2019**, *9*, 010701.
(82) Lai, H.; Xu, F.; Wang, L. A review of the preparation and application of magnetic nanoparticles for surface-enhanced Raman scattering. *J. Mater. Sci.* **2018**, *53*, 8677−8698.

https://doi.org/10.1021/acsomega.2c00058
ACS Omega 2022, 7, 10539−10549